PSFC/JA-00-17

Observations of Cold, High Density Plasma in the Private Flux Region of the Alcator C-Mod Divertor

C.J. Boswell, J.L. Terry, B. LaBombard,
B. Lipschultz, J.A. Goetz

July 2000

Plasma Science and Fusion Center
Massachusetts Institute of Technology
Cambridge, MA 02139 USA

This work was supported by the U.S. Department of Energy, Cooperative Grant No. DE-FC02-99ER54512. Reproduction, translation, publication, use and disposal, in whole or in part, by or for the United States government is permitted.

Submitted for publication to *Journal of Nuclear Materials.*

Observations of Cold, High Density Plasma in the Private Flux Region of the Alcator C-Mod Divertor

C. J. Boswell, J. L. Terry, B. LaBombard, B. Lipschultz, and J. A. Goetz

M. I. T. Plasma Science and Fusion Center
175 Albany Street, Cambridge, MA 02139 USA

Abstract

Significant plasma density has been observed in the private flux zone of the Alcator C-Mod tokamak. The behavior of the D_γ emission profiles is consistent with the source of the plasma being due to an $\vec{E}\times\vec{B}$ drift generated by a poloidal temperature gradient. The plasma flux due to this drift is derived and evaluated. A plasma flux into the private flux zone is inferred by measurements of volumetric recombination using a tangentially viewing CCD camera and several spectroscopic views observing the high n-lines of the D^o Balmer series. For the case of an attached divertor the inferred plasma flux to the PFZ has a linear scaling with respect to plasma pressure, as is expected from the temperature-gradient-induced, $\vec{E}\times\vec{B}$ drift.

Key words: ExB drift, Alcator C-Mod, Divertor Spectroscopy, Recombination
PACS:

1 Introduction

Alcator C-Mod is a high magnetic field, high density, compact tokamak, with a parallel heat flux to the divertor as high as 600 MWm^{-2}.[1] The tokamak is operated in a single lower null magnetic configuration. The data presented here are from a series of experiments where argon and krypton were puffed into the vacuum vessel early in the discharge. In all of these shots the density was raised during the discharge (typically $\bar{n}_e = 1.0 \rightarrow 2.5 \times 10^{20}$ m^{-3}). The inner leg of the divertor for these shots is nearly always detached. The outer divertor leg progresses through attached and then increasingly detached conditions (the radiation front moves from the divertor plate to the x-point). The assessment of detached conditions is made by a comparison of pressures from

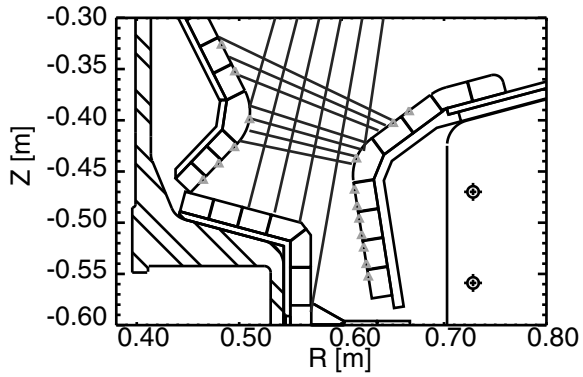

Fig. 1. The triangles are the locations of the flush-mounted probes and the straight lines are the chordal views of the visible spectrometer.

a reciprocating probe scanning the main plasma scrape-off-layer (SOL) and Langmuir probes which are flush-mounted in the divertor plates.[2]

Deuterium line radiation, specifically D_γ ($n = 5 \rightarrow 2$ transition), has been observed to be emitting from the private flux zone (PFZ) during diverted operation. The PFZ is the region below the x-point and bounded by the separatrix and the vacuum vessel in Fig. (2). Typically, strong D_γ emission in the divertor region has been associated with detached divertor operation. D_γ emission along with other spectroscopic data are used to measure the volumetric recombination.[3–7]

2 Diagnostics

Three diagnostics were used to obtain the information used in the analysis of the PFZ plasma. The first diagnostic is a set of flush-mounted Langmuir probes on the outer and inner divertor plates.[2] The Langmuir probes are used to determine plasma density and temperature in both the common flux zone (CFZ) and the PFZ at the divertor plates. The locations of the probes are shown in Fig. (1) by green triangles.

The second diagnostic used is a CCD camera filtered for D_γ emission and viewing the entire divertor tangentially. Calibrated brightness images recorded by the camera are inverted using tomography and the assumption of the toroidal symmetry of D_γ emission to yield 2D emission profiles. The profiles are found to be in agreement with the chord-integrated D_γ measurements made by the visible spectrometer.

The third diagnostic is a visible spectrometer with multiple views of the divertor. The chordal views used of the visible spectrometer are shown in Fig. (1). The spectrometer is used to measure the temperature and density

of the plasma in the regions of brightest emission. The density is determined by measuring the Stark broadening of the $p = 6, 7, 8 \rightarrow 2$ deuterium lines where p is the principle quantum. The temperature is determined by using the knowledge that the population densities of deuterium atoms with energy levels greater than $p = 5$ are in Saha equilibrium and therefore have the temperature dependent distribution of

$$n_p \propto \frac{p^2}{T_e^{3/2}} \exp\left(\frac{13.6}{T_e p^2}\right), \tag{1}$$

where n_p is the population density of electrons in level p and T_e is the electron temperature in eV.[8]

The spectral data recorded by a visible spectrometer are line integrations through different divertor regions. The temperature and density measurements can be spatially localized by recognizing that most of the line integrated brightness comes from the region where the emission is greatest. Thus, the distribution of the emission determines how well localized the measurement is. For brevity the chordal measured n_e and T_e have been attributed to the peak in the emission along the viewing chord. Terry, *et al.*,[9] discusses and defines the number of recombinations per D_γ photon concept that is used here to determine the rate of volume recombination. The recombinations per D_γ photon curves show a strong temperature dependence to T_e for $T_e \leq 0.8$eV, but a less than linear dependence upon n_e.

Using the D_γ emission profile from Fig. (2), the temperature and density measurements from the visible spectrometer, and the recombinations per D_γ photon curves, the recombinations per unit volume per unit time has been measured and summed over the PFZ volume only. Therefore the total recombinations in the PFZ are determined as a function of time. If we assume that all of the plasma particles that enter the PFZ volumetrically recombine, we can relate this measurement to the total plasma particle current into the PFZ.

3 Observations

As the density is increased, four distinct D_γ profile distributions are observed. These are shown in Fig. (2). The first, Fig. (2a), occurs when the density is low and the inner nose is completely detached. There is only D_γ emission on the inner nose, with no emission in the PFZ or along the outer leg. The second, Fig. (2b), is at a somewhat higher density and shows that the emission on the outer nose is decreased and a significant amount of emission comes from the PFZ, with still no emission in the CFZ of the outer leg. The third case, Fig. (2c), is the initially detached case where the outer leg CFZ has a small but

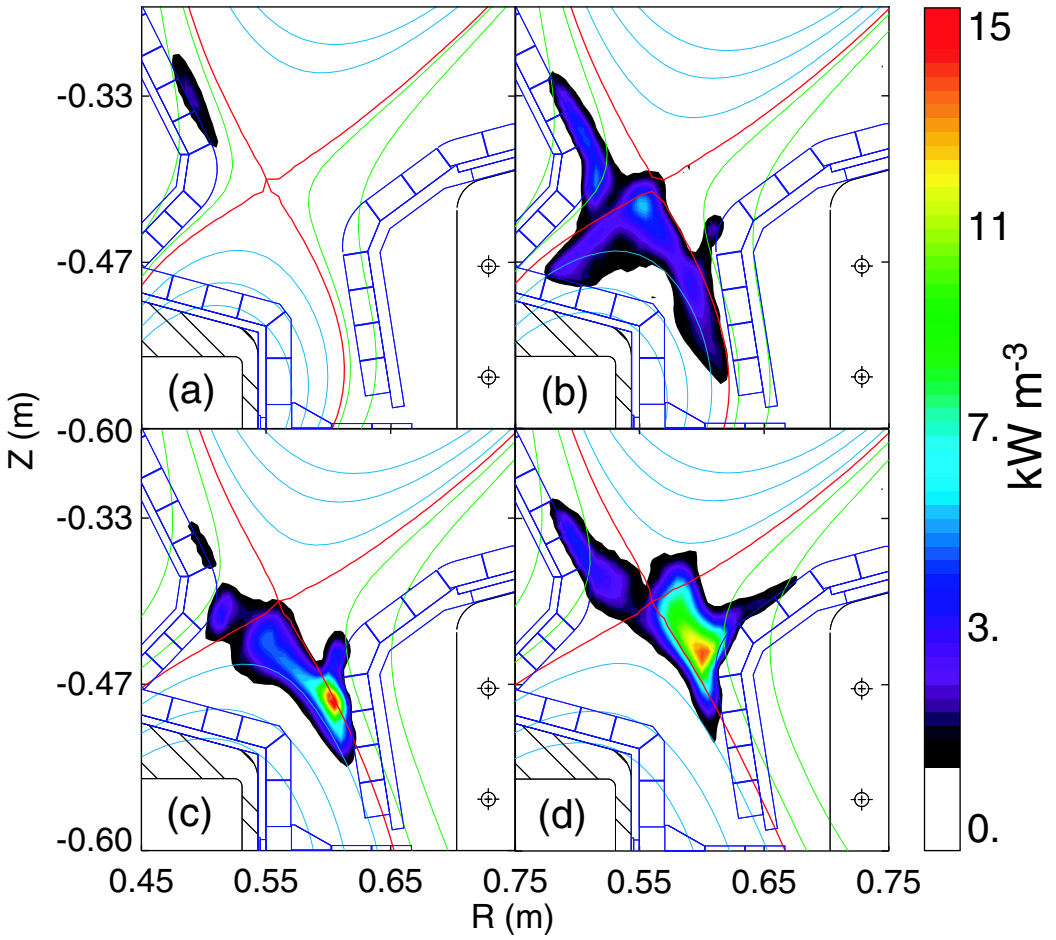

Fig. 2. Four D_γ emission profiles as the $\bar{n}_e$ increases (a) $\bar{n}_e = 1.16 \times 10^{20}$ m^{-3}, (b) $\bar{n}_e = 1.66 \times 10^{20}$ m^{-3}, (c) detachment starts, $\bar{n}_e = 1.86 \times 10^{20}$ m^{-3}, and, (d) expanded detachment front, $\bar{n}_e = 2.30 \times 10^{20}$ m^{-3}.

intense region of emission located at the strikepoint, and the PFZ emission has decreased somewhat from Fig. (2b). In this case the inner nose emission changes very little when compared to Fig. (2b). The final case, Fig. (2d), shows a region of detachment extending along the outer divertor leg, All of the measured D_γ emission is on the outer leg extending to the x-point. The red lines in Fig. (2) indicate the separatrix.

4 Derivation of radial drift

We hypothesize that the flux of plasma into the PFZ is due to a drift generated by a temperature gradient in the poloidal direction. This drift has been discussed in previous articles[10–13] to explain the in/out asymmetry of tokamak divertors. A brief derivation of the radial drift is given below.

From the momentum conservation equation from Braginskii[14],

$$m_e n_e \frac{d\vec{v}_e}{dt} = -\nabla \mathsf{P}_e - e n_e \left(\vec{E} + \vec{v}_e \times \vec{B}\right) + \vec{R}. \tag{2}$$

By neglecting the electron inertia term ($m_e \to 0$) and assuming a scalar pressure, Eq. (2) is reduced to

$$0 = -\nabla p_e - e n_e \left(\vec{E} + \vec{v}_e \times \vec{B}\right) + \vec{R}, \tag{3}$$

where

$$\vec{R} = -\frac{m_e n_e}{\tau_e}\left(0.51 u_{||}\hat{\vec{b}} + \vec{u}_\perp\right) - 0.71 n_e \hat{\vec{b}} \cdot \nabla T_e - \frac{3}{2}\frac{n_e}{\omega_e \tau_e}\hat{\vec{b}} \times \nabla T_e \tag{4}$$

is the momentum exchange term due to friction between the two species for a hydrogenic plasma, $\hat{\vec{b}}$ is the unit vector parallel to the magnetic field, $\vec{u} = \vec{v}_e - \vec{v}_i$, ω_e is the electron cyclotron frequency, and τ_e is the inverse electron-ion collision frequency. Figure (3) shows the coordinate system used for this analysis. The s-direction is parallel to the magnetic field, w-direction is perpendicular to the magnetic field but on the flux surface, and the r-direction is normal to the magnetic flux surface. The toroidal component of Eqs. (3) and (4) with the assumption of toroidal symmetry ($\partial/\partial\phi = 0$) is

$$\begin{aligned} 0 = & -e n_e E_\phi + e n_e v_{er} B_\theta - \frac{m_e n_e}{\tau_e} u_\phi + 0.49 \frac{m_e n_e}{\tau_e}\frac{B_\phi}{B} u_s \\ & -0.71 n_e \frac{B_\phi}{B}\frac{\partial T_e}{\partial s} - \frac{3}{2}\frac{B_\theta}{B}\frac{n_e}{\omega_e \tau_e}\frac{\partial T_e}{\partial r}, \end{aligned} \tag{5}$$

where ϕ represents the toroidal direction and θ represents the poloidal direction. Solving Eq. (5) for v_{er} yields

$$\begin{aligned} v_{er} = & \frac{E_\phi}{B_\theta} - \frac{m_e}{e^2 n_e}\frac{1}{\tau_e B_\theta} J_\phi - 0.49 \frac{m_e}{e \tau_e B_\theta}\frac{B_\phi}{B} u_s + 0.71 \frac{B_\phi}{B}\frac{1}{e B_\theta}\frac{\partial T_e}{\partial s} \\ & + \frac{3}{2}\frac{1}{eB}\frac{1}{\omega_e \tau_e}\frac{\partial T_e}{\partial r}, \end{aligned} \tag{6}$$

where $J_\phi = -e n_e u_\phi$. u_s and the temperature gradient can be reduced to toroidal and poloidal projections using toroidal symmetry and the assumption that there is no poloidal current in this region ($u_\theta = 0$). Therefore Eq. (6) can be written as,

$$v_{er} = \frac{E_\phi}{B_\theta} + \frac{m_e}{e^2 n_e}\frac{1}{\tau_e B_\theta}\left[1 - 0.49\alpha^{-1}\right] J_\phi + 0.71\alpha^{-1}\frac{1}{eB_\phi}\frac{\partial T_e}{\partial \theta}$$

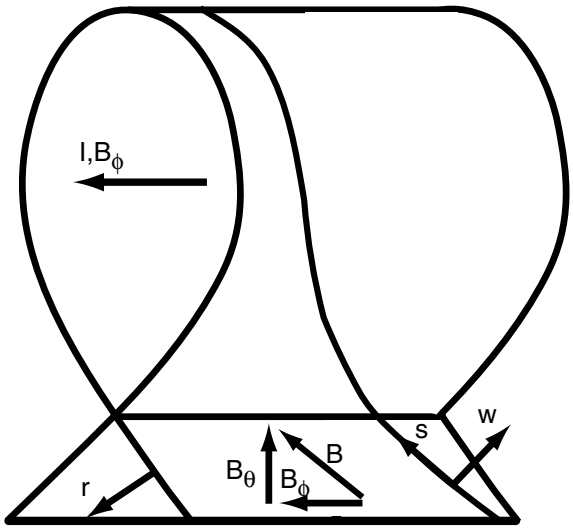

Fig. 3. Coordinate system used in the derivation of the thermoelectric radial drift.

$$+\frac{3}{2}\frac{1}{eB_\phi}\alpha^{-\frac{1}{2}}\frac{1}{\omega_e\tau_e}\frac{\partial T_e}{\partial r}, \tag{7}$$

where $\alpha = \left(1 + B_\theta^2/B_\phi^2\right)$. Since, $\alpha \approx 1$,

$$v_{er} \approx \frac{E_\phi}{B_\theta} + 0.51\frac{m_e}{e^2 n_e}\frac{1}{\tau_e B_\theta}J_\phi + 0.71\frac{1}{eB_\phi}\frac{\partial T_e}{\partial\theta} + \frac{3}{2}\frac{1}{eB_\phi}\frac{1}{\omega_e\tau_e}\frac{\partial T_e}{\partial r}. \tag{8}$$

A similar derivation can be done for the ions and yields the same result.

Of the four terms in Eq. (8) the third term is dominant. The toroidal electric field and current contributions should nearly cancel. For the fourth term to be on the order of the third the radial temperature gradient must be $\approx 10^5$ times steeper than the poloidal temperature gradient. As will be seen, in the cases of interest it is typically only ten times higher. Therefore the radial drift is dominant and will be dealt with exclusively,

$$v_{er} \approx 0.71\frac{1}{eB_\phi}\frac{\partial T_e}{\partial\theta}. \tag{9}$$

This means that the existence of a poloidal temperature gradient on the outer leg from the X-point to the strikepoint leads to a radially inward drift of plasma into the PFZ.

5 Qualitative Analysis

The agreement between the hypothesis that the drift is due to poloidal temperature gradient and the observations can be seen beginning with the first case, Fig. (2a), where the inner nose is detached and the outer nose is attached. The temperature gradient is shallow ($50 \rightarrow 25$ eV) and the density is low enough along the outer leg create only a weak flux of particles ($\sim 10^{20}$ particles $s^{-1)}$) entering the PFZ . With this weak flux of particles the density in the PFZ cannot rise to the level required for volumetric recombination to be evident by strong D_γ emission, and no D_γ emission is seen. In the second case, Fig. (2b), can be described as high-recycling; pressure is constant on a flux surface but, not poloidal density and temperature. Therefore there should be plasma in the PFZ, and it is observed. The third case, Fig. (2c), is the partially detached case. Here the pressure is not constant, but modeling shows that the gradients still exist below the x-point to the detachment front.[15] In such a case, it is expected that the plasma will flow into the PFZ only above this sharp gradient region and not below it. This is what is observed in Fig. (2c). In last case, Fig. (2d), the region of sharp temperature gradient has moved all the way to the x-point. There is only a shallow gradient along the outer leg. This yields no flow from the outer leg into the PFZ. Instead, in this case the poloidal gradient will drive a flow into the core directly above the x-point. As the density increases, the flux into the core above the x-point increases, and a cold MARFE forms above the x-point eventually leading to a disruption. This is seen on Alcator C-Mod.[6,7]

The distribution of the D_γ emission does not agree with the possibility of perpendicular *diffusion* being the dominant mechanism fueling the PFZ. If diffusion was the main cause of particle flux into the PFZ one would expect the particle flux to increase when the divertor detachment is extended to the x-point due to the large perpendicular density gradient formed on the outer leg. This is not observed and therefore cross-field diffusion is not considered to be the dominant mechanism.

6 Quantitative Analysis

The total number of particles per second that drift into the private flux region is

$$I_e = \int n_e v_{er}\, dA, \tag{10}$$

where $\int \ldots dA$ is the integral over the total area of the outer leg. By substituting Eq. (9) into Eq. (10) and recognizing that in a tokamak $B_\phi = B_o R_o / R$, where B_o and R_o are the magnetic field and radial position of the center of the main plasma, the particle current into the PFZ can be written as

$$I_e \approx \frac{1.42\pi}{eB_o R_o} \int_{\mathrm{sp}}^{\mathrm{x}} n_e R^2 \frac{\partial T_e}{\partial \theta}\, d\theta, \tag{11}$$

where sp is the strikepoint, x is the x-point. In the attached case ($\partial p_e / \partial s = 0$) this integral can be approximated as,

$$I_e \approx \frac{1.42\pi R^2 p_e}{eB_o R_o} \ln\left(\frac{T_{\mathrm{X}}}{T_{\mathrm{sp}}}\right) \tag{12}$$

assuming the variation in R^2 is small enough to remove it from inside the integral.

Using the assumption that all plasma particles that enter the PFZ volumetrically recombine in the PFZ and using the approximations that yielded Eq. (12), the relation between the PFZ recombination rate and the particle current into the PFZ is

$$\left(\frac{\partial N_e}{\partial t}\right)_{\mathrm{recomb}} \approx \beta p_e, \tag{13}$$

where

$$\beta = \frac{1.42\pi R^2}{eB_o R_o} \ln\left(\frac{T_{\mathrm{X}}}{T_{\mathrm{sp}}}\right). \tag{14}$$

Figure (4) shows the comparison of the PFZ recombination rate as a function of peak plasma pressure on the outer leg for the discharge shown in Fig. (2). The linear dependence is what is expected from Eq. (13).

The line shown in Fig. (4) is a linear regression fit of the data. This yields a slope of 6.3×10^{18} recombinations s^{-1} Pa^{-1} with an R^2 value of 0.826. Given that $R \approx 0.6\mathrm{m}$, $B_o = 5.4\mathrm{T}$, and $R_o = 0.67\mathrm{m}$ and if $ln\left(T_{\mathrm{X}}/T_{\mathrm{sp}}\right) \approx 2.25$ then, the slope is the same as predicted from Eq. (14).

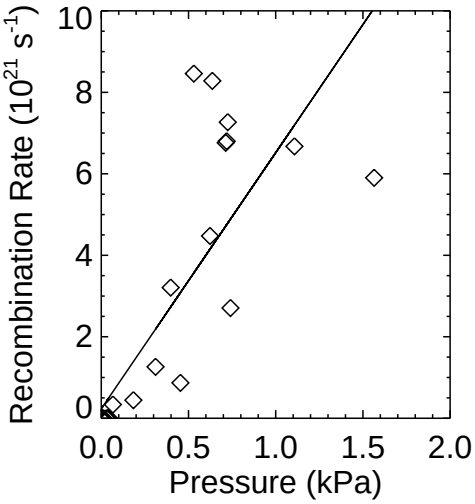

Fig. 4. A plot of the PFZ recombination rate as a function of the peak electron pressure on the outer leg when the outer leg was attached for the shot in Fig. (2).

7 Discussion and Summary

D_γ emission shows the existence of plasma in the private flux zone of the Alcator C-Mod tokamak. Using spectroscopic measurement we observe that there is a significant recombination rate in this region, which is likely fed by cross-field transport from across the separatrix. From Braginskii's equations, a radial drift is derived to explain the behavior of the PFZ plasma. The dominant drift is due to a poloidal temperature gradient. This mechanism for the flux into the PFZ is consistent with the observed behavior of the plasma.

In the attached case the flux into the PFZ is linear with the plasma pressure and logarithmic with respect to the ratio of x-point temperature to temperature at the divertor plate. This linear behavior is observed and verified on Alcator C-Mod.

As the line averaged density is increased the outer divertor leg becomes detached and a sharp poloidal temperature gradient is located at or slightly above the x-point, thus reducing the flow into the PFZ. As the density is increased further plasma flows into the x-point from the CFZ due to the local temperature gradient. This cools the plasma on the closed flux surfaces enough to generate an x-point MARFE, which subsequently leads to disruption. This has been observed on the Alcator C-Mod tokamak.[6,7]

8 Acknowledgements

The authors would like to thank the Alcator C-Mod group for assistance in acquiring these data. The authors would also like to extend there gratitude to Prof. P. C. Stangeby for his helpful discussions on the topic of the $\vec{E} \times \vec{B}$ drift. This work was supported by the U. S. Dept. of Energy under grant #DE-FC02-99ER54512.

References

[1] I. H. Hutchinson *et al.*, Physics of Plasmas **1**, 1511 (1994).

[2] B. LaBombard *et al.*, Journal of Nuclear Materials **220–222**, 976 (1995).

[3] G. M. McCracken *et al.*, Nuclear Fusion **38**, 619 (1998).

[4] G. M. McCracken *et al.*, Journal of Nuclear Materials **266–269**, 37 (1999).

[5] M. E. Fenstermacher *et al.*, Journal of Nuclear Materials **266–269**, 348 (1999).

[6] B. Lipschultz *et al.*, Journal of Nuclear Materials **266–269**, 370 (1999).

[7] B. Lipschultz *et al.*, Physics of Plasmas **6**, 1907 (1999).

[8] B. Lipschultz *et al.*, Physical Review Letters **81**, 1007 (1998).

[9] J. L. Terry *et al.*, Physics of Plasmas **5**, 1759 (1998).

[10] F. L. Hinton and G. M. Staebler, Nuclear Fusion **29**, 405 (1989).

[11] G. M. Staebler, Nuclear Fusion **31**, 729 (1991).

[12] A. V. Chankin *et al.*, Plasma Phys. Control. Fusion **36**, 1853 (1994).

[13] P. C. Stangeby and A. V. Chankin, Nuclear Fusion **36**, 839 (1996).

[14] S. I. Braginskii, *Reviews of Plasma Physics* (Consultants Bureau, New York, 1965), Vol. 1.

[15] F. Wising *et al.*, Contributions to Plasma Physics **36**, 136 (1996).